Modelling of an Offshore Multi – Purpose Floating Structure Supporting a Wind Turbine Including Second – Order Wave Loads

T.P. Mazarakos[#1], D.N. Konispoliatis[#2], D.I. Manolas[*3], S.G. Voutsinas[*4], S.A. Mavrakos[#5]

[#]*Laboratory for Floating Structures and Mooring Systems, School of Naval Architecture and Marine Engineering*
National Technical University of Athens (NTUA)
9 Heroon Polytechneiou Str., GR15780, Athens, Greece

[1]tmazarakos@naval.ntua.gr

[2]dkonisp@naval.ntua.gr

[5]mavrakos@naval.ntua.gr

[*]*Aerodynamic Laboratory, School of Mechanical Engineering*
National Technical University of Athens
9 Heroon Polytechneiou Str., GR15780, Athens, Greece

[3]manolasd@fluid.mech.ntua.gr

[4]spyros@fluid.mech.ntua.gr

***Abstract*— This paper summarizes the coupled hydro–aero–elastic analysis behind the modelling of a multi–purpose floating structure suitable for offshore wind and wave energy sources exploitation, built to incorporate properly, the solutions of the diffraction and the pressure– and motion– dependent radiation problems around the floating structure and the aerodynamics of the Wind Turbine (W/T) in the frequency and the time domain. The floating structure, under the action of regular surface waves, encompasses an array of hydrodynamically interacting Oscillating Water Column (OWC) devices consisting of concentric vertical cylinders, moored through tensioned tethers as a tension leg platform (TLP) supporting a 5 MW W/T. Numerical results concerning the motions of the floating structure are presented for two water depths at 120m and 200m, whereas, in addition, for the 120m water depth case the mean second order loads are given as well.**

***Keywords*— Multi-purpose floating structure, Oscillating water column device, Wind turbine, Second–order wave loads**

I. INTRODUCTION

In the last few years growing interest in developing multi-purpose offshore renewable energy devices is taking place worldwide. The main challenge for these devices is to absorb not only wave but also the wind energy ([1], [2]). The main disadvantage of wave power, as with the wind from which it originates, is its random variability in several time–scales, thus semi–submersible platforms for electricity generation from the combined wind and wave action could be more effective than wave energy converters (WEC) alone. Due to technological similarities to onshore wind energy, the offshore wind industry is developing quickly. Moreover, as far as the analysis of such multi–purpose structures is concerned, recent investigations concerning their numerical and experimental modelling have been presented in the literature ([3], [4]).

In the present contribution we consider a system of three identical OWC devices which are placed at the corners of a triangular floater that supports a 5MW W/T. The geometric configuration of each OWC device consists of a partially immersed toroidal oscillating chamber of finite volume that is formed between an exterior cylindrical shell and a concentric interior truncated cylinder, where the TLP tethers are mounted on. (Figs.1,2). The wave action causes the captured water column to oscillate in the annular chamber, compressing and decompressing the air above the inner water surface. In the centre of the platform a solid cylindrical body is arranged in order to support a horizontal – axis W/T at the top of a tower. Detailed data are given in [5] and [6]. The tower of the WT is cantilevered at an elevation of 10m above the sea water level (SWL) to the top of the main column of the floating platform.

Fig.1. Multi-purpose floating structure with three OWC devices and a W/T (image above water surface)

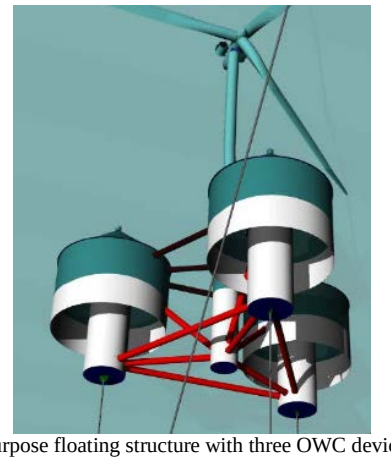

Fig.2. Multi-purpose floating structure with three OWC devices and a W/T (image bellow water surface)

The floating structure is exposed to the combined wind and wave action in 120m and 200m depth waters as an extension of [7] where only the water depth of 200m was studied. The tendons stiffness is considered different in the two water depth cases. Furthermore the mean drift forces of the floating structure are estimated in frequency domain and the difference frequency quadratic hydrodynamic forces are introduced in the time domain solution using Newman's approximation.

II. FORMULATION OF THE PROBLEM

A. Calculation of the velocity potential function

We consider that the multi–body system is excited by a plane periodic wave of amplitude H/2, frequency ω and wave number k propagating in water of finite water depth. The distance between each OWC device is L=50m. The outer and inner radii of each device's chamber q, q=1, 2, 3, are denoted by α_q, b_q, respectively (α_q=14.05m, b_q=14m), whereas the distance between the bottom of the q device and the sea bed is denoted by h_q=112m for water depth 120m and h_q=192m for water depth 200m. The radius of the interior concentric cylindrical body in each device q, is denoted by $b_{1,q}$=5m and the distance between its bottom and the sea bed is $h_{1,q}$=100m and $h_{1,q}$=180m for water depth 120m and 200m, respectively. The radius of the central cylindrical body that supports the W/T is c=3.25m and the distance between its bottom and the sea bed is h_c=100m and h_c=180m for water depth 120m and 200m, respectively (Fig.3 & Fig.4).

Small amplitude waves, inviscid, incompressible and irrotational flow are assumed, so that linear potential theory can be employed. A global Cartesian co–ordinate system O–XYZ with origin on the sea bed and its vertical axis OZ directed positive upwards and coinciding with the vertical axis of symmetry of the central body is used. Moreover, three local cylindrical co-ordinate systems (r_q, θ_q, z_q), q = 1, 2, 3 are defined with origins on the sea bottom and their vertical axes pointing upwards and coinciding with the vertical axis of symmetry of the q device.

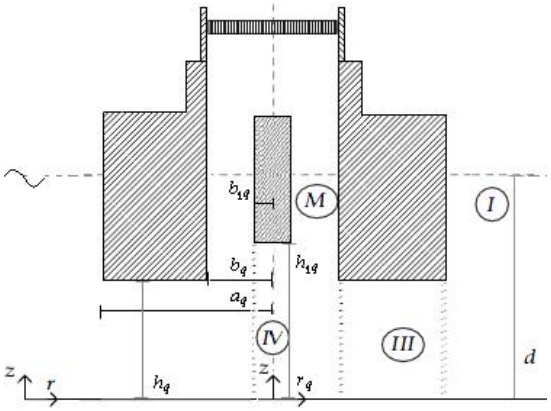

Fig.3. Definition sketch of the q OWC device of the array

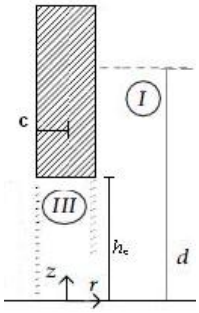

Fig. 4. Definition sketch of the central cylindrical body basing the W/T

The fluid flow around the q = 1, 2, 3, 4 device/body (three OWCs & one solid body) can be described by the potential function:

$$\Phi^q\left(r_q,\theta_q,z;t\right)=\mathrm{Re}\left\{\phi^q\left(r_q,\theta_q,z\right)\cdot e^{-i\omega t}\right\} \qquad (1)$$

Following [8] the spatial function ϕ^q can be decomposed, on the basis of linear modelling, as:

$$\phi^q=\phi_0^q+\phi_7^q+\sum_{p=1}^{4}\sum_{j=1}^{6}\dot{x}_{j0}^p\cdot\phi_j^{qp}+\sum_{i=1}^{3}P_{in0}^i\cdot\phi_P^{qi} \qquad (2)$$

Here, ϕ_0^q is the velocity potential of the undisturbed incident harmonic wave [9]; ϕ_7^q is the scattered potential around the q device/body, when it is considered fixed in waves with the duct open to the atmosphere, so that the pressure in the chamber is equal to the atmospheric one (for the OWCs); ϕ_j^{qp} is the motion–dependent radiation potential around the device/body q resulting from the forced oscillation of the p–th device/body, p=1,2,3,4, moving with unit velocity amplitude, $\dot{x}_{j0}^p$, with $\dot{x}_j^p=\mathrm{Re}\left\{\dot{x}_{j0}^p\cdot e^{-i\omega t}\right\}$; ϕ_P^{qi} is the pressure–dependent radiation potential around the q–th device/body, due to unit time harmonic oscillating pressure head, $P_{in}^i=\mathrm{Re}\left\{p_{in0}^i\cdot e^{-i\omega t}\right\}$, in the chamber of the i=1,2,3 device which is considered fixed in otherwise calm water.

The velocity potential of the undisturbed incident wave system, propagating at angle β, with respect to the positive x–axis can be expressed in the cylindrical co–ordinate frame of the q–th body as follows [9]:

$$\phi_0^q(r_q,\theta_q,z) = -i\omega\frac{H}{2}\sum_{m=-\infty}^{\infty} i^m \Psi_{0,m}^q(r_q,z)\cdot e^{im\theta_q} \qquad (3)$$

where

$$\frac{1}{d}\Psi_{0,m}^q(r_q,z) = e^{ik\ell_{oq}\cos(\theta_{oq}-\beta)}\frac{Z_0(z)}{d\cdot Z_0'(d)}J_m(kr_q)\cdot e^{-im\beta} \qquad (4)$$

The symbols used above are defined in Fig. 3. Here J_m is the m–th order Bessel function of first kind and $Z_0(z)$ is defined by:

$$Z_0(z) = \left[0.5\left[1+\sinh(2kd)/(2kd)\right]\right]^{-1/2}\cdot\cosh(kz) \qquad (5)$$

with $Z_0'(d)$ being its derivative at $z = d$. Frequency ω and wave number k are related by the dispersion equation.

The diffraction, i.e. $\phi_D^q = \phi_0^q + \phi_7^q$, q=1,2,3,4, the motion–dependent radiation potentials around the isolated q device/body and the pressure– dependent radiation potential around the isolated q device, when it is considered alone in the field, are expressed in its own cylindrical co–ordinate system (r_q,θ_q,z) as follows:

$$\phi_D^q(r_q,\theta_q,z) = -i\omega\frac{H}{2}\sum_{m=-\infty}^{\infty} i^m \Psi_{D,m}^q(r_q,z)\cdot e^{im\theta_q} \qquad (6)$$

$$\phi_j^{qq}(r_q,\theta_q,z) = -i\omega\sum_{m=-\infty}^{\infty} \Psi_{j,m}^{qq}(r_q,z)\cdot e^{im\theta_q} \qquad (7)$$

$$\phi_P^{qq}(r_q,\theta_q,z) = \frac{1}{i\omega\rho}\sum_{m=-\infty}^{\infty} \Psi_{P,m}^{qq}(r_q,z)\cdot e^{im\theta_q} \qquad (8)$$

where ρ is the water density.

The potentials ϕ_j^l ($l \equiv q,\ qp$; j=D, 1, …, 6, P; p, q = 1,2,3,4; i=1,2,3) are solutions of Laplace's equation in the entire fluid domain and satisfy the following boundary conditions:

$$\omega^2\phi_j^l - g\frac{\partial\phi_j^l}{\partial z} = \begin{cases} 0 & \text{for } r_q \ge a_q;\ \text{or } r_q \ge c \\ & l \equiv q,\ j = D;\quad \text{or} \\ & l \equiv qp,\ j = 1,2,...,6,\ P \\ 0 & \text{for } b_{1,q} \le r_q \le b_q; \\ & l \equiv q,\ j = D;\quad \text{or} \\ & l \equiv qp,\ j = 1,2,...,6 \\ -\delta_{q,i}\dfrac{i\omega}{\rho} & \text{for } b_{1,q} \le r_q \le b_q; \\ & l \equiv qi;\ j = P \end{cases} \qquad (9)$$

on the outer and inner free sea surface $(z = d)$, and the zero normal velocity on the sea bed $(z = 0)$. Moreover, the potentials have to fulfil kinematic conditions on the mean device/body's wetted surface. Finally, a radiation condition must be imposed which states that propagating disturbances must be outgoing.

The unknown potential functions $\Psi_{j,m}^{k,l}$, k=*I*, *III*, *M*, *IV* (see Eq.6– Eq.8) can be established in each fluid region surrounding the q–th device/body (see Figs. 3 and 4) using the method of matched axisymmetric eigenfunction expansions.

Next, the potentials, ϕ_j^{qp}, ϕ_P^{qi}, (j=1, …, 6) around the body q of the multi– body configuration due to oscillation of body p, p=1,2,3,4, in otherwise still water (motion– dependent radiation potential) or due to inner time harmonic oscillating pressure head in the air chamber of the device i, i=1,2,3, (pressure– dependent radiation potential), can be expressed in the q–th body's cylindrical coordinate system, as:

$$\phi_j^{qp}(r_q,\theta_q,z) = -i\omega\sum_{m=-\infty}^{\infty} \Psi_{j,m}^{qp}(r_q,z)\cdot e^{im\theta_q} \qquad (10)$$

$$\phi_p^{qi}(r_q,\theta_q,z) = \frac{1}{i\omega\rho}\sum_{m=-\infty}^{\infty} \Psi_{p,m}^{qi}(r_q,z)\cdot e^{im\theta_q} \qquad (11)$$

In order to express the potentials, ϕ_j^{qp}, ϕ_p^{qi} in the form of Eq10 and Eq11, the multiple scattering approach [10], [11] is used. This method has been further elaborated to solve the diffraction and the motion– dependent radiation problems around arbitrarily shaped, floating or/and submerged vertical axisymmetric bodies in [9] and [12] and for the diffraction and the pressure– dependent radiation problems for an interacting array of OWC's devices in [4], thus it will be no further elaborated here.

B. Volume flow

The time dependent volume flow produced by the oscillating internal water surface in q OWC device, q = 1, 2, 3, is denoted by $Q^q(r_q,\theta_q,z,t) = \mathrm{Re}\left[q^q(r_q,\theta_q,z)\cdot e^{-i\omega t}\right]$, where:

$$q^q = \iint_{S_i^q} u_z\, dS_i^q = \iint_{S_i^q}\frac{\partial\phi^q}{\partial z}\, r_q\, dr_q\, d\theta_q \qquad (12)$$

Here u_z denotes the vertical velocity of the water surface, and S_i^q the inner water surface in the q device, q=1, 2, 3.

Assuming that the Wells turbine is placed in a duct between the q device's chamber and the outer atmosphere and that it is characterized by a pneumatic admittance Λ^q, then the total volume flow is equal to [13], [8]:

$$Q^q(t) = \Lambda^q \cdot P_{in}^q(t) \tag{13}$$

with $P_{in}^q(t)$ being the pressure drop in the turbine of the *q* OWC device. Decomposing the total volume flow, q^q, of the *q*–th device, same as for the velocity potential (see Eq2) into three terms associated with the diffraction, q_D^q, and the motion– and pressure– dependent radiation problems, q_R^q, q_P^q, respectively, we can obtained:

$$q^q = q_D^q + q_R^q + \sum_{i=1}^{3} p_{in0}^i \cdot q_P^{qi} \tag{14}$$

Here:

$$q_R^q = \sum_{p=1}^{4}\sum_{j=1}^{6} \dot{x}_{j0}^p \cdot q_{3,j}^p - \dot{x}_{30}^p \cdot S_i^p \tag{15}$$

where S_i^p is the inner water surface in the *p* device, *p*=1, 2, 3.

The pneumatic admittance Λ^q for the OWCs was considered as a real and positive number equal to the optimum coefficient Λ_{opt} of the same restrained OWC device but in isolation condition as in [13].

C. Hydrodynamic forces

The various forces on the *q* device/body can be calculated from the pressure distribution given by the linearized Bernoulli's equation:

$$P(r_q, \theta_q, z, t) = -\rho \frac{\partial \Phi^q}{\partial t} = i\omega\rho\phi^q \cdot e^{-i\omega t} \tag{16}$$

where ϕ^q is the *q* device's velocity potential in each fluid domain *I*, *III*, *M* and *IV* (see Figs. 3 and 4). The horizontal and vertical exciting forces and moments acting on an array of OWC devices have been presented in [4].

The motion – dependent hydrodynamic reaction forces and moments $F_{ij}^{qp}(t)$ acting on the device/ body *q*, *q*=1,2,3,4, in the *i*–th direction due to the oscillation of device/ body *p*, *p*=1,2,3,4, in the *j*–th direction, can be obtained by the linearized Bernoulli's equation (Eq. (16)) as:

$$F_{ij}^{qp}(t) = f_{ij}^{qp} . e^{-i\omega t} = i\omega\rho\dot{x}_{j0}^p \iint_{S_0} \phi_j^{qp} n_i^q dS . e^{-i\omega t}$$

Here, the generalized normal components n_i^q are defined as $\vec{n}^q = (n_1^q, n_2^q, n_3^q)$ and $\vec{r}^q \times \vec{n}^q = (n_4^q, n_5^q, n_6^q)$, with $\vec{r}^q$ being the position vector with respect to the origin of the coordinate system, while, ϕ_j^{qp}, is defined in Eq. (2).

The complex form f_{ij}^{qp} may be recast in the form [14]:

$$f_{ij}^{qp} = \omega^2 (a_{ij}^{qp} + i/\omega\, b_{ij}^{qp}) x_{j0}^p \tag{17}$$

Here, a_{ij}^{qp}, b_{ij}^{qp}, are the well– known added mass and damping coefficients.

In the same way, the hydrodynamic pressure forces and moments $f_{P,i}^{ql}$ acting on the device/body *q* in the *i*–th direction due to oscillating pressure head in the *l*=1,2,3 device can be written in the form:

$$f_{P,i}^{ql} = \left(-e_i^{ql} + id_i^{ql}\right) \cdot p_{in0}^l \tag{18}$$

Here e_i^{ql}, d_i^{ql} are the pressure-induced damping coefficients.

The total hydrodynamic forces on the entire multi– body configuration can be calculated by properly superposing the corresponding forces on each device with respect to the reference point of motion, *G*, of the entire structure (for details see [12]).

D. Mooring system

The floating structure is moored with a TLP mooring system of three tendons spread symmetrically about the platform Z- axis. The body- fixed locations (fairleads) where the mooring tendons attach the platform are located at the base of the offset columns, at a depth of 20 m below the sea water level (SWL). The anchors are located at a water depth of 120m/ 200m below the SWL. Each of the 3 tendons has an unstretched length of 100m (for water depth 120m) and 180m (for water depth 200m), a diameter of 0.130m, an equivalent mass per unit length of 104 kg/m and a submerged weight per unit length equal to 888.6N/m. The pretension of each tendon is assumed constant for the two water depth cases and equal to 10800kN. The mooring line stiffness of each tendon k_{xx} = 108kN/m and k_{zz} = 26533kN/m for water depth 120m and k_{xx} = 60kN/m k_{zz} =14700kN/m, respectively, for water depth 200m. The mooring tendons properties are listed in Table I.

TABLE I
Mooring System properties

Number of Tendons	3	3
Depth to Anchors Below SWL (Water Depth)	120 m	200 m
Depth to Fairleads Below SWL	20 m	20 m
Mooring Line Length, L	100 m	180 m
Mooring Line Diameter, D	130 mm	130 mm
Equivalent Mooring Line Mass Density	104 kg/m	104 kg/m
Equivalent Mooring Line Mass in Water	888.6 N/m	888.6 N/m
Mooring Line stiffness k_{xx} of each tendon = T_{pr}/L	108 kN/m	60 kN/m
Mooring Line stiffness k_{zz} of each tendon = EA/, A=$\pi D^2/4$, E: Yeung's modulus	26533 kN/m	14700 kN/m
Pretension of each tendon, T_{pr}	10800 kN	10800 kN
E.A (KN)	2.653.300	2.653.300

E. Aerodynamic loading

In the frequency domain formulation, the contribution of the W/T is projected on the 6 floater motion. This is carried out in the context of Hamiltonian dynamics with gravity and aerodynamics being the external forcing. The Blade Element Momentum theory defines the aerodynamic loading as a function of the operational conditions and the motions of the floater that change the effective angles of attack seen by the blades. By linearizing all terms with respect to the case of zero floater motions (static equilibrium), additional mass, damping and stiffness matrices are defined which contribute the W/T aerodynamic, inertial-gyroscopic and gravitational loading in the equation of motion (see below equation 19) [15].

F. The time domain problem

The time domain simulations are carried out using the fully coupled hydro-servo-aeroelastic model hydroGAST developed at NTUA [16], [17], [18]. hydroGAST is a multi-body Finite Element Method (FEM) dynamic model of the complete system. The aerodynamic loading is based on a Boundary Element Method (BEM) formulation, the hydrodynamic loading is based on linear potential theory including the quadratic viscous drag term from the Morison's equation and the mooring tendons are modelled as co-rotating non-linear truss elements. The drag coefficient for the evaluation of the quadratic drag in Morison equation was assumed to be equal to 0.6 for the cylindrical columns and 4.8 for the bottom surfaces. Code-to-code verification of hydroGAST has been carried out within the context of the OC4 IEA Annex [19], [20]. In the present work the 2nd order effects have been added. To this end, the mean drift forces and moments have been obtained from the frequency domain solution and the loads corresponding to the frequency difference quadratic terms as defined in Newman's approximation [21] have been added.

III. RESPONSE AMPLITUDE OPERATORS (RAO'S)

The investigation of the dynamic equilibrium of the forces acting on the moored multi – body system (OWC devices and W/T) leads to the following well – know system of differential equations of motions, describing the couple hydro–aero-elastic problem of the investigated moored multi–purpose floating structure in the frequency domain [22]:

$$\sum_{j=1}^{6}\begin{bmatrix} -\omega^2(M_{i,j}+A_{i,j}+M^{WT} \\ +\frac{i}{\omega}B_{i,j}+\frac{i}{\omega}B^{WT}_{i,j}) \\ +C_{i,j}+C^{WT}_{i,j}+C_{mooring} \end{bmatrix}\cdot x_{j0} = \quad (19)$$
$$= F_i + F_{P,i}$$

for i=1,…,6.

where $M_{i,j}$ and $C_{i,j}$ are elements of the (6x6) mass and stiffness matrices of the entire configuration; $A_{i,j}$, $B_{i,j}$, are the hydrodynamic masses and potential damping of the entire configuration; F_i are the exciting forces acting on the multi–body system at the i–th direction; $F_{P,i}$ are the pressure hydrodynamic forces acting on the multi–body system at the i–th direction; X_{j0} is the motion displacement of the entire OWC system at the j–th direction with respect to a global co – ordinate system G; M^{WT}, B^{WT} and C^{WT}, are the mass, damping and stiffness which contribute the W/T aerodynamic, inertial-gyroscopic and gravitational loading respectively, while $C_{mooring}$ is the mooring lines stiffness matrix.

The RAO's can be estimated from time series data from the following equation:

$$RAO(\omega) = \frac{|P_{xy}(\omega)|}{P_{xx}(\omega)} \quad (20)$$

where P_{xx} is the auto power spectral density and P_{xy} is the cross spectral density. x refers to the input (wave elevation) and y to the output (each motion). P_{xx}, P_{xy} are calculated using Welch's method [23] with a sufficient number of data split and 50% overlap between the split data parts. The time domain simulations lasted 3600sec - the first 600sec are excluded – assuming a uniform wind speed and white noise waves of 1m significant wave height.

IV. MEAN AND SLOWLY – VARYING SECOND – ORDER WAVE LOADS

By making use of the momentum conservation principle the expressions for both horizontal and vertical mean drift forces and the corresponding pitching moments are given by [24]:

$$F^{(2),q} = \rho\iint_{S_R}\left\{\left[\Phi_t^q+\frac{1}{2}\nabla\Phi^q.\nabla\Phi^q+gz\right]\mathrm{n}-\frac{\partial\Phi^q}{\partial n}\nabla\Phi^q\right\}dS -$$
$$-\mathrm{k}\rho\iint_{S_B}\left[\Phi_t^q+\frac{1}{2}\nabla\Phi^q.\nabla\Phi^q\right]dS-\mathrm{k}\rho g\iint_{S_{FS}\cup S_0^q} zn_z dS \quad (21)$$

$$M^{(2),q} = \rho\iint_{S_R}\left\{\left[\Phi_t^q+\frac{1}{2}\nabla\Phi^q.\nabla\Phi^q+gz\right]\left(\mathrm{x}\times\mathrm{n}\right)-\left(\mathrm{x}\times\nabla\Phi^q\right)\frac{\partial\Phi^q}{\partial n}\right\}dS -$$
$$-\rho\iint_{S_B}\left[\Phi_t^q+\frac{1}{2}\nabla\Phi^q.\nabla\Phi^q\right]\left(y\mathrm{i}-x\mathrm{j}\right)dS -$$
$$-\rho g\iint_{S_{FS}\cup S_0^q} z\left[(yn_z-zn_y)\mathrm{i}+(zn_x-xn_z)\mathrm{j}\right]dS \quad (22)$$

Here, time averages over right hand side of the above equations are understood, **k**, **i** and **j** are the unit vectors in z–, x– and y–axes respectively, **n** is the unit normal vector oriented outwards from the fluid control volume, **x** is the position vector of a point on the control surfaces with respect to the coordinate system of the examined device and the assumption was made that the sea bottom is horizontal. Moreover, S_B is the sea bottom, S_{FS} the portion of the free surface enclosed between S_0^q, and the fixed vertical cylindrical control surface S_R surrounding each device/body of the array, which in the present contribution it is assumed to coincide in the radial direction with the mean wetted surface of each device.

The complete representation of the velocity potential around the device/body has to be taken into account by including both wave-like and evanescent wave modes [24]. Drift loads on the individual devices are properly superimposed with respect to a global co-ordinate system in order to evaluate the drift loads on the entire multi-body configuration considered as a unit.

Having calculated the mean second-order drift loads in regular waves, the time history of the slowly-varying second-order force $F_x^{(2)}(t)$ can be approximated using the Newman's relation [21]:

$$F^{(2)}(t) = \left|L^{(+)}(t)\right|^2 - \left|L^{(-)}(t)\right|^2 \quad (23)$$

where:

$$L^{(\pm)}(t) = \mathrm{Re}\left\{\sum_m^{\infty} A_m e^{i(\omega_m t+\varphi_m)}\left[\pm 2R(\omega_m)\right]^{\frac{1}{2}}\right\} \quad (24)$$

The signs in (24) have been introduced for the case that the quantity under the square root is negative. Moreover,

$$A_m = \left\{2S_\zeta(\omega_m)d\omega\right\}^{\frac{1}{2}} \quad (26)$$

where $S_\zeta(\omega)$ is the wave spectrum at the installation site, φ_m arbitrary phase angle associated with the wave frequency ω_m and $R(\omega_m) = F^{(2)}{}_{x_0}(\omega_m)/(H/2)^2$ is the mean drift force in regular waves, see Eqs. (21) – (22), pro square of wave amplitude for a wave frequency ω_m.

V. NUMERICAL RESULTS

A. Eigen values

In Table II the first 12 eigenvalues of the coupled system are presented, as provided by hydroGAST for both water depths. In the flex case, the flexibility of the W/T's members (tower, shaft, blades) is considered, while in the rigid case the members are stiff.

As expected, the frequencies of the floater's rigid motions are higher at the water depth of 120m compared to the depth of 200m, due to the increased stiffness of the tendons (see table I).

The main differences, between the rigid and the flex case for both depths, are: the reduction of the roll/pitch natural frequencies from 0.42Hz to 0.3Hz at 120m and from 0.3Hz to 0.25Hz at 200m, as well as the presence of the tower fore-aft and side-to-side frequencies at ~1.02Hz and ~0.85Hz respectively. Flexibility is important in the TLP case due to the strong coupling between the roll/pitch motion and the side-to-side/fore-aft bending moments of the tower. The modes of the blades and of the drive train (shaft) are not coupled with the motions of the floater, so they remain almost unchanged in the two water depths and not expected to appear in the RAOs of the floater motions.

It is noted that for stable TLP design, the surge, sway and yaw natural frequencies should be less than 0.05Hz and the heave, roll and pitch frequencies should be above 0.2 to 0.25Hz, which is the frequency range of a common wave spectrum.

TABLE II
Coupled system eigen values [Hz]

	Depth 120m		**Depth 200m**	
Mode description	**flex**	**rigid**	**flex**	**rigid**
Platform Surge	0.042	0.042	0.026	0.026
Platform Sway	0.042	0.042	0.026	0.026
Platform Yaw	0.044	0.044	0.028	0.028
Platform Roll	**0.294**	**0.419**	**0.244**	**0.301**
Platform Pitch	**0.296**	**0.420**	**0.245**	**0.301**
Platform Heave	0.821	0.824	0.569	0.569
1st Drive train Torsion	0.599	-	0.585	-
1st Blade Flapwise Yaw	0.635	-	0.634	-
1st Blade Flapwise Pitch	0.665	-	0.653	-
1st Blade Collective Flap	0.708	-	0.702	-
1st Tower Fore-Aft	**1.016**	-	**0.854**	-
1st Tower Side-Side	**1.024**	-	**0.861**	-

B. RAO's

In previous works [25], [7] it was concluded that the RAO's were consistently predicted by the frequency and time domain methods. The main difference was observed in the roll and the pitch RAO's which was attributed to the absence of coupling between these two motions with the tower bending modes in the frequency domain method, as long as the flexibility of the system is not included. In the present paper, the RAO's predicted by the time domain method are presented for two water depths at zero wind speed (and no rotation) and at the rated wind speed of 11.4m/s for zero wave heading angle.

The change in depth leads to different stiffness of the tendons and by that to frequency shifts in the RAOs. The natural frequencies of table II are clearly depicted in figures 5 to 10. Since the wave is considered propagating along the longitudinal (surge) direction, the lateral motions sway and roll are less excited and only through couplings. The aerodynamic influence is clearly seen in the reduction of the pitch motion at the natural frequency (Fig. 9) and in the increase of the yaw motion due to the gyroscopic effect (Fig. 10). At 120m depth the heave amplitude is reduced and in turn the OWC is expected to produce more energy (Fig. 7), while the roll and the pitch natural frequencies are well above the wave frequency range.

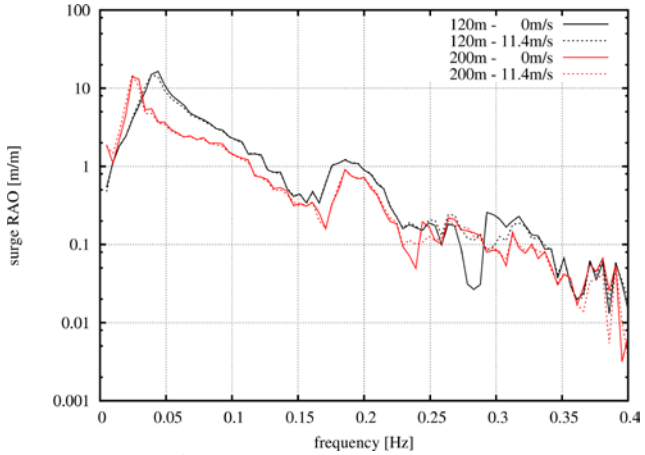

Fig. 5. Surge RAO for 120m and 200m water depth at 0m/s and 11.4 m/s wind speeds.

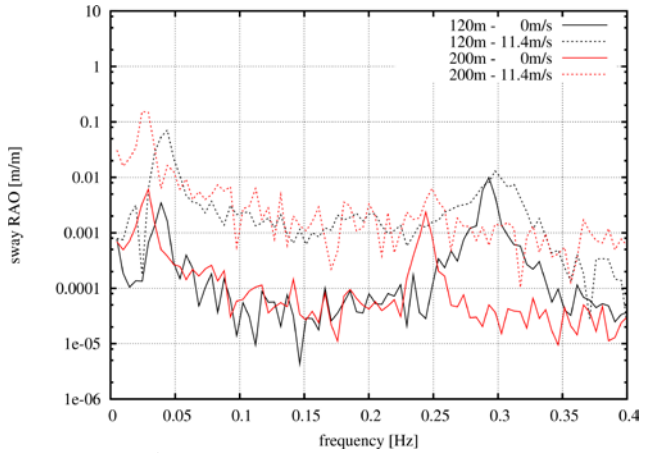

Fig. 6. Sway RAO for 120m and 200m water depth at 0m/s and 11.4 m/s wind speeds.

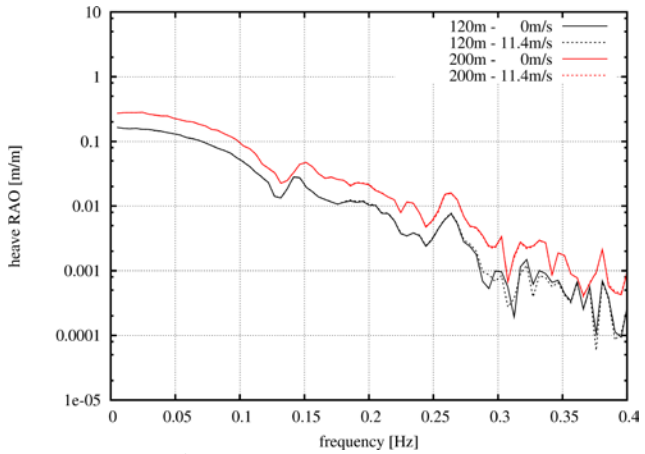

Fig. 7. Heave RAO for 120m and 200m water depth at 0m/s and 11.4 m/s wind speeds.

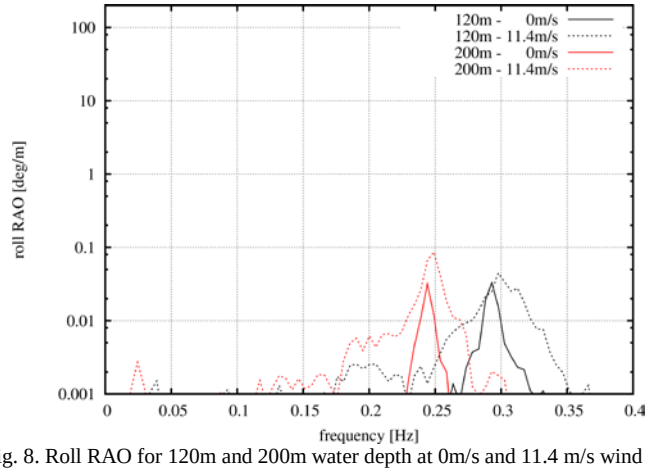

Fig. 8. Roll RAO for 120m and 200m water depth at 0m/s and 11.4 m/s wind speeds.

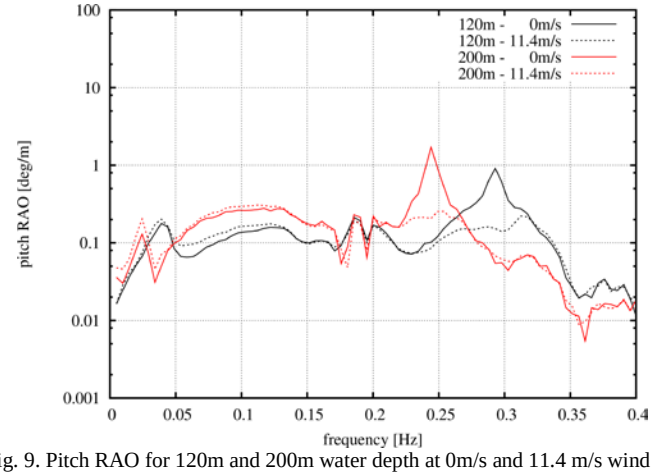

Fig. 9. Pitch RAO for 120m and 200m water depth at 0m/s and 11.4 m/s wind speeds.

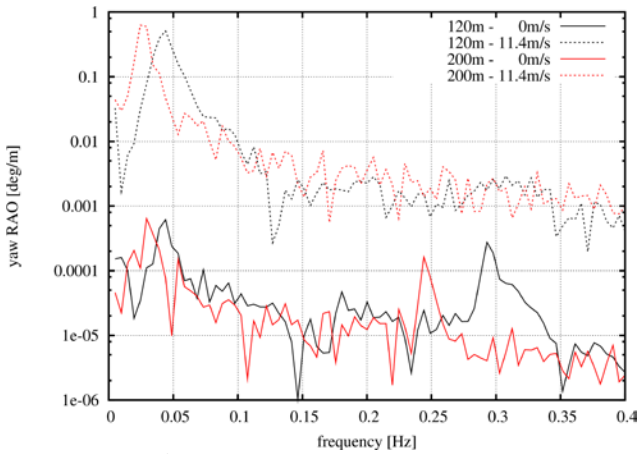

Fig. 10. Yaw RAO for 120m and 200m water depth at 0m/s and 11.4 m/s wind speeds.

C. Mean surge and sway drift forces and yawing moment

The steady drift forces are plotted in Figs. 11 to 13 as a function of the incident wave frequency (rad/s) and are rendered dimensional for atmospheric air pressure inside the air chambers. Each graph includes results for the surge, sway and yaw motions for four wave headings, 0, 30, 60 and 90 degrees respectively. The water depth is 120m. The surge drift force in Fig. 11 increases when the wave heading decreases. The opposite happens for the sway drift forces in Fig. 12. In Fig.13 it is depicted that the yaw moments for 30 and 90 degrees are symmetrical, due to symmetry of the floating structure every 120deg.

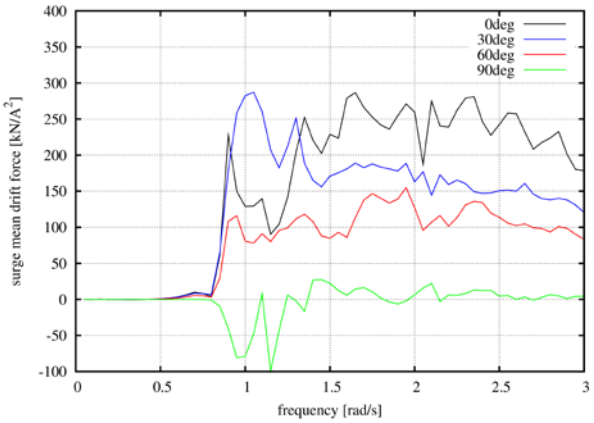

Fig. 11. Surge mean drift force of the floating structure at 120m depth for 0°, 30°, 60° and 90° wave heading angles.

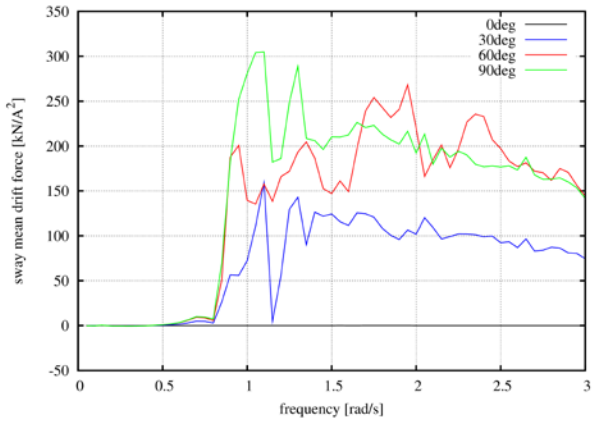

Fig. 12. Sway mean drift force of the floating structure at 120m depth for 0°, 30°, 60° and 90° wave heading angles.

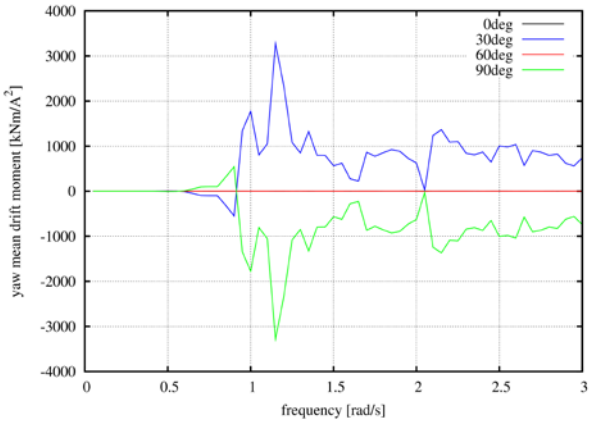

Fig. 13. Yaw mean drift moment of the floating structure at 120m depth for 0°, 30°, 60° and 90° wave heading angles.

D. Linear vs Newman's approximation

In order to identify the importance of the 2nd order wave hydrodynamic loads on the behaviour of the present TLP floating wind turbine designs, two normal turbulence load cases are simulated, corresponding to wind speeds 11.4m/s (rated) and 18m/s respectively. Newman' approximation for the evaluation of the second – order forces has been used. The runs correspond to cases with the 2nd order loads (Newman) and without (linear). By anticipating that differences will appear in case of high wave amplitudes, in both simulations the sea state is defined by a Jonswap wave spectrum with significant wave height equal to 9m and peak period equal to 12sec with wave heading angle 30°, at 120m water depth.

As expected, the consideration of the second – order difference frequency loads increases the mean values of the surge and the sway motions, as presented in table III for both wind speeds. The similar standard deviations justify that the general behaviour of the floating structure is not affected by the inclusion of the 2nd order hydrodynamic loads and also explain the increase of the maximum values, caused by the increased mean positions. The heave, roll and pitch motions remain almost unchanged and so are not presented.

In Fig. 14 the Power Spectral Density (PSD) of the first-order exciting force is compared against the PSD of the second-order difference-frequency load from the Newman's approximation in the surge direction. Although the 2nd order wave force in the wider range of wave frequencies is 3 to 4 orders less compared to its first–order counterpart, in the low frequency regime becomes higher than the 1st order force. That is why the surge and the pitch motions at low frequencies are increased when 2nd order hydrodynamic loads are included (Figs. 15 and 16). As far as particularly the pitch motion is concerned (Fig.16), it has to be pointed out that the second order contributions are solely due to surge-pitch couplings, i.e. no mean second-order pitch moment has been considered in the present formulation. The yaw motion is less affected by the 2nd order yawing moment as shown in Fig. 17. However, the differences in the PSD's of the surge and pitch motions at low frequencies due to second – order wave effects seem to be not important in calculating the total induced loads on the W/T, as the latter differ by less than 0.5% when compared to their counterparts obtained on the basis of linear wave loading (not presented in the paper for the sake of space economy). This behaviour can be traced back to the fact that the low-frequency spectral wave energy content is approximately two orders of magnitude lower than its maximum at ~0.08Hz. The latter however, dictates the dynamic loads on the W/T due to the wave action.

TABLE III
Statistics comparison of surge, sway and yaw motions.

	11.4 m/s					
	Linear			**Newman**		
	max	**mean**	**std**	**max**	**mean**	**std**
Surge [m]	12.24	2.13	4.10	12.94	2.81	4.13
Sway [m]	6.47	0.23	2.45	6.72	0.50	2.46
Yaw [deg]	7.46	0.14	2.42	7.26	0.23	2.44
	18 m/s					
Surge [m]	11.77	1.41	4.10	12.38	2.09	4.14
Sway [m]	6.46	0.21	2.47	6.71	0.48	2.48
Yaw [deg]	7.17	-0.03	2.42	7.06	0.06	2.43

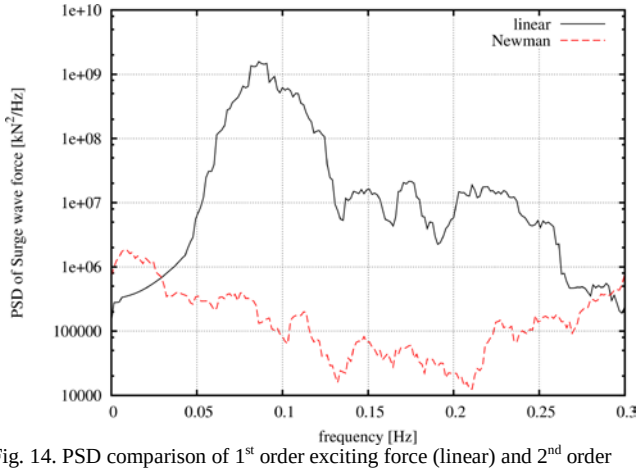

Fig. 14. PSD comparison of 1st order exciting force (linear) and 2nd order difference frequency force from Newman's approximation in surge direction.

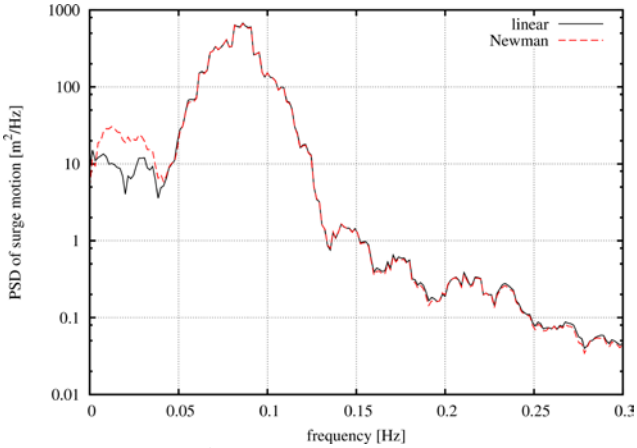

Fig. 15. PSD comparison of the surge motion with and without the inclusion of the 2nd order difference frequency force from Newman's approximation for 11.4m/s wind speed. Note that above 0.06 Hz the two PSDs are identical.

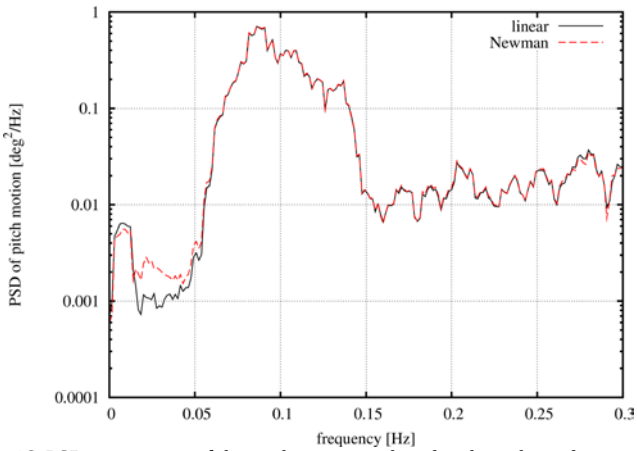

Fig. 16. PSD comparison of the pitch motion with and without the inclusion of the 2nd order difference frequency force from Newman's approximation for 11.4m/s wind speed. Note that above 0.06 Hz the two PSDs are identical.

Inclusion of the full difference-frequency quadratic terms could further increase the differences, as is also indicated in [26], for a spar buoy floater though. Also the sum-frequency second – order terms could be of significance in the TLP case in studying especially the tendons fatigue life.

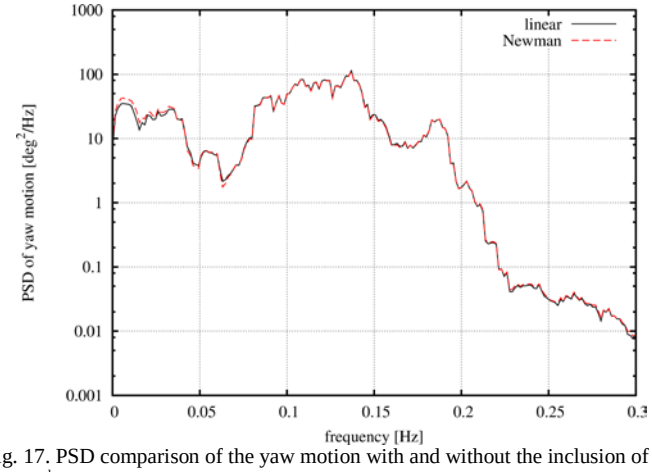

Fig. 17. PSD comparison of the yaw motion with and without the inclusion of the 2nd order difference frequency force from Newman's approximation for 11.4m/s wind speed. Note that above 0.06 Hz the two PSDs are identical.

VI. CONCLUSIONS

A TLP floater supporting the National Renewable Energy Laboratory (NREL) 5MW WT and 3 OWC devices has been analyzed. If the flexibility of the tower is considered the roll and the pitch natural frequencies are reduced and the tower mode is also depicted in the corresponding RAOs. For this design, RAO's of the complete system have been calculated using time domain simulations for water depths of 120m and 200m at zero and rated wind speed. The aerodynamic damping reduces the pitch RAO, while the gyroscopic effects increase the yaw RAO. Differences with respect to the water depth are linked to the different stiffness of the tendons. Moreover numerical results concerning the mean drift loads exerted on the floating structure for the 120m water depth case are calculated in the frequency domain using the momentum conservation principle. The mean drift loads are then used by the time domain method in order to include the 2nd order difference frequency loads using Newman's approximation. The influence of the second-order loads is visible in the PSD of the surge and the sway motions for low frequencies from 0 to 0.06 Hz. In most of the relative figures, the first-order results (linear - black solid line) are below the ones obtained by including the second-order difference-frequency wave excitation (Newman - red dashed line). However, the effect of the low - frequency second-order motion components on the induced loads on the W/T seems to be not important in the particular design as the latter differ by less than 0.5% compared to their linear counterparts. Thus, the consideration of the 2nd order hydrodynamic difference – frequency loading terms in evaluating the coupled dynamic behavior of the proposed TLP design seems to be not important.

ACKNOWLEDGMENT

This research has been co-financed by the European Union (European Social Fund– ESF) and Greek national funds through the Operational Program "Education and Lifelong Learning" of the National Strategic Reference Framework (NSRF) 2007– 2013: Research Funding Program: ARISTEIA, Program POSEIDON (2041).

REFERENCES

[1] A. Aubault, M. Alves, A. Sarmento, D. Roddier, A. Peiffer, "Modeling of an oscillating water column on the floating foundation WINDFLOAT," in *Proc. 30th International Conference on Ocean, Offshore and Arctic Engineering (OMAE2011)*, Rotterdam, The Netherlands, 2011.

[2] S.A. Mavrakos, I.K. Chatjigeorgiou, T. Mazarakos, D.N. Konispoliatis, A. Maron, "Hydrodynamic forces and wave run-up on concentric vertical cylinders forming piston-like arrangements," in *Proc. The 26th International Workshop on Water Waves and Floating Bodies (IWWWFB 2011)*, Athens, Greece, 2011.

[3] J.R. Nader, S.P. Zhu, P. Cooper, B. Steppenbelt, "A finite element study of the efficiency of arrays of oscillating water column wave energy converters," *J. Ocean Engineering*, vol. 43, p. 72–81, 2012.

[4] D.N. Konispoliatis, S.A. Mavrakos, "Hydrodynamics of arrays of OWC's devices consisting of concentric cylinders restrained in waves," in *Proc. 10th European Wave and Tidal Energy Conference (EWTEC 2013)*, Aalborg, Denmark, 2013.

[5] J. Jonkman, S. Butterfield, W. Musial and G. Scott, "Definition of a 5-MW Reference Wind Turbine for Offshore System Development," Technical Report, NREL/TP-500-38060, USA, 2009.

[6] J. Jonkman, "Definition of the Floating System for Phase IV of OC3," Technical Report NREL/TP-500-47535, USA, 2010.

[7] T.P. Mazarakos, D.N. Konispoliatis, D.I. Manolas, S.G. Voutsinas, S.A. Mavrakos, "Coupled Hydro – Aero – Elastic Analysis of a Multi – Purpose Floating Structure for Offshore Wind and Wave Energy Sources Exploitation," in *Proc. The 12th International Conference on the Stability of Ships and Ocean Vehicles (STAB 2015)*, Glasgow, Scotland, UK, 2015 (accepted).

[8] J. Falnes, *Ocean waves and oscillating systems: linear interactions including wave-energy extraction*; Cambridge University Press, 2002.

[9] S.A. Mavrakos & P. Koumoutsakos, "Hydrodynamic interaction among vertical axisymmetric bodies restrained in waves," J. *Applied Ocean Research*, vol. 9, No. 3, 1987.

[10] V. Twersky, "Multiple scattering of radiation by an arbitrary configuration of parallel cylinders," *J. Acoustical Soc. of America*, vol. 24 (1), 1952.

[11] M. Okhusu, "Hydrodynamic forces on multiple cylinders in waves," *Int. Symp. on the Dynamics of Marine Vehicles and structures in Waves*, University College London, London, 1974.

[12] S.A. Mavrakos. "Hydrodynamic coefficients for groups of interacting vertical axisymmetric bodies," *J. Ocean Engineering*, vol. 18, No. 5, p. 485–515, 1991.

[13] D.V. Evans, R. Porter, "Efficient calculation of hydrodynamic properties of OWC type devices," in *Proc. 15th International Conference on Ocean, Offshore and Arctic Engineering (OMAE 1996)*, vol. I–Part B, p. 123–132, 1996.

[14] J.N. Newman, "The motions of a floating slender torus," *J. Fluid Mech*, vol. 83, p. 721–735, 1977.

[15] G. Papadakis, V. Riziotis, S. Voutsinas, S.A. Mavrakos, "*W/T's reduced order aeroelastic models (in Greek)*," Technical Report No. D3.2, Program POSEIDON (2014), Greek General Secretariat for Research and Technology, 2014.

[16] V.A. Riziotis, S.G. Voutsinas, "GAST: A general aerodynamic and structural prediction tool for wind turbines," in *Proc. European Wind Energy Conference (EWEC 1997)*, Dublín, Ireland, 1997.

[17] V. Riziotis, S.G. Voutsinas, E.S. Politis, P.K. Chaviaropoulos, "Aeroelastic Stability of Wind Turbines: the problem, the methods, the issues," in *Proc. Wind Energy*, 7, p. 373–392, 2004.

[18] D. Manolas, V. Riziotis, S. Voutsinas, "Assessment of 3D aerodynamic effects on the behaviour of floating wind turbines," *The science of making torque from Wind, TORQUE 2012*, Oldenbourg, Germany, 2012.

[19] J. Jonkman, A. Robertson, W. Popko, F. Vorpahl, A. Zuga, M. Kohlmeier, T.J. Larsen, A. Yde, K. Saetrrtro, K.M. Okstad, J. Nichols, T.A. Nygaard, Z. Gao, D. Manolas, K. Kim, Q. Yu, W. Shi, H. Park, A.V. Rojas,J. Dubois, D. Kaufer, P. Thomassen, M.J. de Ruiter, J.M. Peeringa, H. Zhiwen, H.von Waaden, "Offshore Code Comparison Collaboration Continuation (OC4), Phase I – Results of Coupled Simulations of an Offshore Wind Turbine with Jacket Support Structure," in *Proc. International Offshore and Polar Engineering Conference* (*ISOPE 2012)*, Rhodes, Greece, 2012.

[20] A. Robertson, J. Jonkman, F. Vorpahl, W. Popko, J. Qvist, L. Froyd, X. Chen, J. Azacona, E. Uzungoglu, C. Guedes Soares, C. Luan, H. Yutong, F. Pengcheng, A. Yde, T. Larsen, J. Nichols, R. Buils, J. Lei, T. Andres Nygard, D. Manolas, A. Heege, S. Ringdalen Vatne, H. Ormberg, T. Duarte, C. Godreau, H. Fabricius Hansen, A. Wedel Nielsen, H. Riber, C. Le Cunff, R. Abele, F. Beyer, A. Yamaguchi, K. Jin Jung, H. Shin, W. Shi, H. Park, M. Alves and M. Guerinel, "Offshore code comparison collaboration, continuation within IEA wind task 30: phase II results regarding a floating semisubmersible wind system," in *Proc. 33rd International Conference on Ocean, Offshore and Arctic Engineering (OMAE 2014), San Francisco, USA*, 2014.

[21] J.N. Newman, "Second-order, Slowly-varying Forces on Vessels in Irregular Waves," in *Proc. International Symposium on Dynamics of Marine Vehicles and Structures in Waves*, London, 1974.

[22] T.P. Mazarakos, S.A. Mavrakos, D.N. Konispoliatis, S.G. Voutsinas, D. Manolas, "Multi- purpose floating structures for offshore wind and wave energy sources exploitation," in *Proc. COCONET Workshop for Offshore Wind Farms in the Mediterranean and Black Seas*, Anavyssos- Greece, 9- 10 June 2014.

[23] P.D. Welch, "The Use of Fast Fourier Transform for the Estimation of Power Spectra: A Method Based on Time Averaging Over Short, Modified Periodograms," *IEEE Transactions on Audio Electroacoustics*, AU-15, p.70–73, 1967.

[24] S.A. Mavrakos, "Mean drift loads on multiple vertical axisymmetric bodies in regular waves," in *Proc. 5th International Offshore and Polar Engineering Conference (ISOPE 1995)*, The Hagen, The Netherlands, Vol. **3**, p. 547-555, 1995.

[25] T.P. Mazarakos, D.I. Manolas, T. Grapsas, S.A. Mavrakos, V.A. Riziotis, S.G. Voutsinas, "Conceptual design and advanced hydro-aero-elastic modeling of a TLP concept for floating wind turbine applications," in *Proc. International Conference on Renewable Energies Offshore* (*RENEW 2014), Lisbon, Portugal*, 2014.

[26] T. Duarte, A. Sarmento and J. Jonkman, "Effects of Second-Order Hydrodynamic Forces on Floating Offshore Wind Turbines," NREL/CP-5000-60966. Golden, CO: National Renewable Energy Laboratory, p. 18. Accessed November 3, 2014.